Scientific Reports

https://doi.org/10.1038/s41598-026-45771-z

Article in Press

Synthesis, SAR, and multi-target evaluation of isonicotinoyl hydrazones as potent MPO/AChE inhibitors and metal chelators for Alzheimer's disease

Received: 3 January 2026

Accepted: 22 March 2026

Published online: 03 April 2026

Cite this article as: Wei Z., Liu Z., Chang Y. *et al.* Synthesis, SAR, and multi-target evaluation of isonicotinoyl hydrazones as potent MPO/AChE inhibitors and metal chelators for Alzheimer's disease. *Sci Rep* (2026). https://doi.org/10.1038/s41598-026-45771-z

Zeyang Wei, Zhenguo Liu, Ying Chang, Zixiao Wang, Bo Guo, Xiaojiao Ma & Kai Zhao

Synthesis, SAR, and Multi-target Evaluation of Isonicotinoyl Hydrazones as Potent MPO/AChE Inhibitors and Metal Chelators for Alzheimer's Disease

Zeyang Wei,*[a] Zhenguo Liu,[a] Ying Chang,[a] Zixiao Wang,[b] Bo Guo,[a] Xiaojiao Ma[a] and Kai Zhao*[a]

ABSTRACT:

Isonicotinoyl hydrazone derivatives (**1-20**) were synthesized and evaluated for their inhibitory activities against myeloperoxidase (MPO) and acetylcholinesterase (AChE), antioxidant activity, metal ion chelation, regulation of reactive oxygen species (ROS), and cytoprotective activity, with the aim of identifying multi-target therapeutic candidates for Alzheimer's disease. In this study, **9** exhibited a free radical scavenging activity of 93% and showed strong inhibitory effects against MPO and AChE, with inhibition rates of 90% and 73%, respectively. An in-depth structure–activity relationship (SAR) analysis revealed that **9** possesses a favorable pharmacological balance between lipophilicity and electronic properties. Moreover, **9** effectively chelated Cu^{2+}, Fe^{2+}, Mg^{2+}, and Zn^{2+} ions. It also reduced oxidative stress, significantly improved cell viability in neuronal damage models, and prevented cell death in a concentration-dependent manner.

Furthermore, molecular docking studies demonstrated that **9** exhibits favorable binding affinities toward both target enzymes, providing a structural basis for its dual-target inhibitory activity and supporting the rationality of the structure–activity relationship analysis. Collectively, these results suggest that **9** represents a potential therapeutic candidate for the development of therapeutic agents for Alzheimer's disease.

Key words: Isonicotinoyl hydrazone, Antioxidant. Acetylcholinesterase, Myeloperoxidase, Biometal chelation, Molecular docking.

Department of Pharmacy, Northwest Woman's and Children's Hospital, Xi'an, China.
b. Department of Pharmacy, Honghui Hospital, Xi'an Jiaotong University, Xi'an, China.
*Correspondence: Zeyang Wei, Email: zeyangwei22@163.com; Kai Zhao, Email: zhka47@163.com

1. Introduction

Alzheimer's disease (AD) is the most common age-related neurodegenerative disease, and cognitive and neuropsychiatric symptoms ultimately lead to the loss of behavioral capacity in patients.[1] The neuropathological features of AD include amyloid angiopathy, significant neuroinflammation, extracellular beta amyloid protein (Aβ) deposition, intracellular neurofibrillary tangles (NFTs), and loss of neuronal processes and synapses.[2,3] These pathological features, including amyloid fiber deposition associated with senile plaques and the accumulation of abnormal tau protein filaments, lead to the resulting loss of nerve fiber tail neurons and synapses, glial cell activation, and inflammation.[4] However, the exact pathogenic mechanism remains unclear, which has led to the proposal of many

overlapping hypotheses, including the amyloid cascade hypothesis, Tau protein hypothesis, metal ion hypothesis, inflammation hypothesis, and oxidative stress hypothesis.[5]

Isoniazid is a known anti tuberculosis drug,[6] and its hydrazide functional group is an excellent metal chelating agent.[7] Isoniazid can chelate with some metals that exacerbate AD to alleviate symptoms.[8] Furthermore, cholinergic dysfunction is a classic feature of AD, making acetylcholinesterase (AChE) inhibition a primary symptomatic target. (Ref to AChE) And oxidative stress is an important step in the pathogenesis of AD. It can damage biomolecules such as proteins, DNA, and lipids, thereby accelerating cancer, aging, inflammation, cardiovascular and neurodegenerative diseases. Common oxidative stress substances such as reactive oxygen species (ROS). The sources of ROS include redox active metals, mitochondria, and enzymes such as NADPH oxidase and myeloperoxidase (MPO).[9-11] The main product of MPO is hypochlorous acid (HOCl), which is an extremely oxidizing substance. The increase of these two substances in neurodegenerative diseases can lead to severe tissue damage.[12] Therefore, successfully protecting neuronal cells from oxidative damage may potentially prevent AD.[13] Based on this multifactorial rationale, we have designed a series of Isonicotinoyl hydrazone derivatives to achieve therapeutic goals by concurrently modulating multiple pathological processes of AD (i.e, AChE and oxidative stress targets like MPO). In recent years, hydrazone-based derivatives have remained a focal point in multi-target-directed ligands (MTDLs) design for AD, with numerous studies exploring their role in inhibiting MAO-B, modulating Aβ aggregation, and acting as neuroprotective metal-chelating agents.[14-16] While these reports highlight the versatility of the hydrazone moiety, the simultaneous targeting of the MPO-mediated oxidative pathway alongside AChE inhibition remains a less explored but highly promising frontier.

Building upon these recent advancements, while various hydrazone scaffolds are known in the literature for their basic activities, the unique significance of this article lies in establishing the specific and potent potential of isonicotinoyl hydrazones as integrated multitarget anti-AD agents. Unlike many recent hydrazone MTDLs that focus on the AChE/BACE1 or AChE/MAO-B axes,[15] our series is characterized by a robust dual-action profile: potent acetylcholinesterase (AChE) inhibition combined with excellent antioxidant capacity (via ROS and MPO scavenging). This simultaneous modulation of cholinergic and oxidative stress pathways offers a crucial therapeutic advantage over current single-target therapies.[16]

To tackle the multifactorial nature of AD, we adopted MTDLs strategy based on the pharmacophore hybridization approach. Our design strategy (**Scheme 1**) integrates two essential pharmacophores: (1) The Metal-Chelating & Radical Scavenging Unit: We selected the isoniazid scaffold as the foundational core. The resulting acylhydrazone linkage (–CO–NH–N=CH–) serves as a multidentate coordination site, capable of sequestering redox-active metals (Cu^{2+}, Fe^{2+}). Furthermore, the N-H group of the acylhydrazone moiety acts as a potential hydrogen donor to neutralize free radicals. (2) The Hydrophobic & Enzyme Binding Unit: To enhance binding affinity to the active sites of AChE and MPO, we incorporated diverse aromatic aldehydes chosen to interact with the hydrophobic pockets of

these enzymes. Specifically, we constructed a focused library of derivatives to systematically explore structure-activity relationships (SAR): bulky hydrophobic substituents were introduced to engage the Catalytic Anionic Site (CAS) of AChE through π-π stacking interactions with key aromatic residues, while various electron-donating or electron-withdrawing groups were added to fine-tune the lipophilicity-electronic balance, thereby optimizing MPO inhibitory potency and overall molecular lipophilicity.

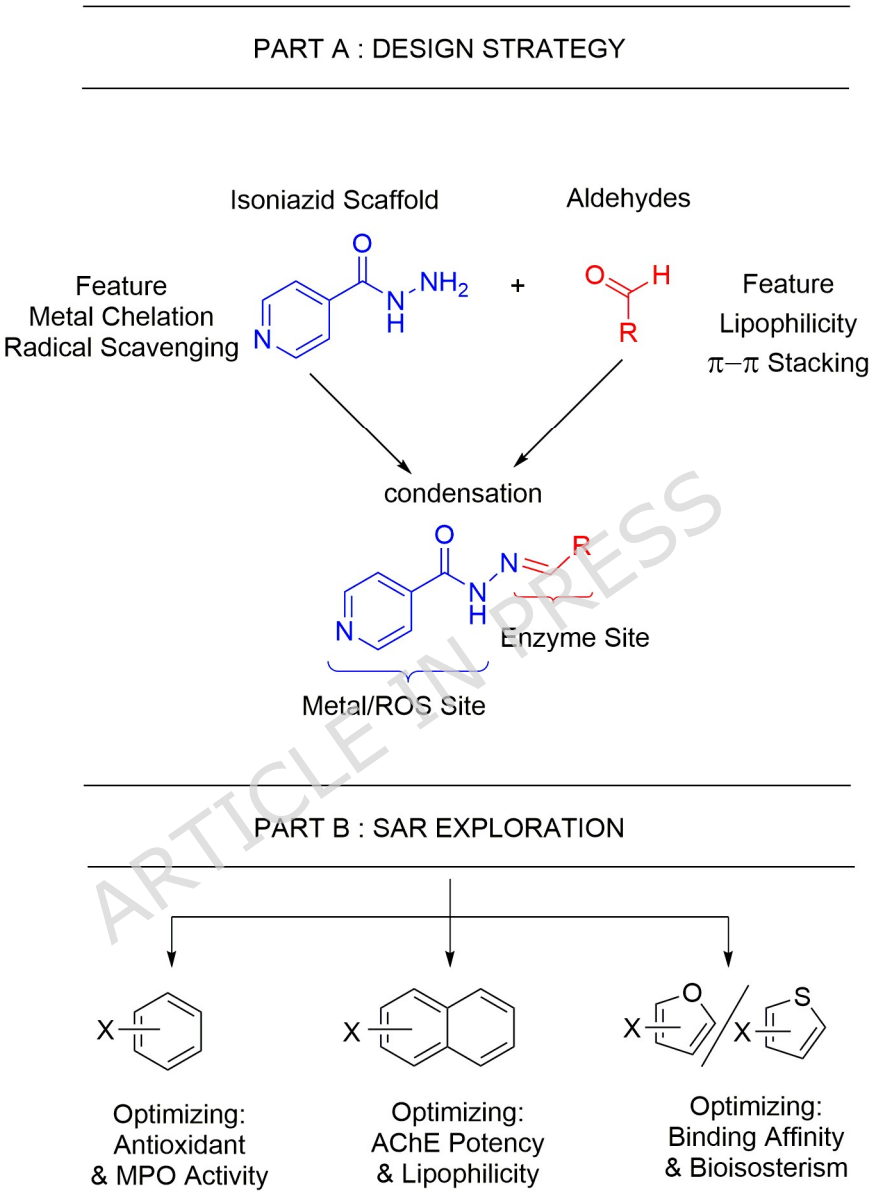

Scheme 1. Design strategy of novel isonicotinoyl hydrazone derivatives as multi-target-directed ligands (MTDLs) for AD. The strategy combines the metal-chelating/antioxidant pharmacophore of isoniazid (blue) with hydrophobic aromatic moieties (red) **.** to simultaneously target metal chelation, oxidative stress, AChE, and MPO.

Herein, we report the synthesis, *in vitro* multi-target evaluation, and SAR analysis of this new series of isonicotinoyl hydrazones. We identify a lead

compound and use molecular docking studies to fully rationalize the mechanism of its promising multitarget activity.

2. Results and discussion

2.1 Chemical synthesis

The targeted Isonicotinoyl hydrazone derivatives (**D**) were synthesized *via* a straightforward and robust sequence, as depicted in **Scheme 2**. The synthetic route initiated with the methyl esterification of commercially sourced isonicotinic acid (**A**). This transformation was efficiently carried out using methanol as both solvent and reactant, in the presence of a catalytic amount of concentrated sulfuric acid, providing methyl isonicotinate (**B**) in excellent yield after purification. In the subsequent step, the key pharmacophore, Isonicotinoyl hydrazone (**C**) was generated by treating ester B with a molar excess of hydrazine hydrate in ethanol. This hydrazinolysis reaction proceeded smoothly under reflux conditions, affording Isonicotinoyl hydrazone in high purity. The final library of **D** was prepared by reacting **C** with a structurally diverse array of aldehydes. To systematically investigate the influence of the substituent on biological activity, the aldehydes were strategically selected to constitute two main series: **Series I** encompassed benzaldehyde derivatives bearing various electron-donating or electron-withdrawing groups on the phenyl ring. **Series II** was designed to include aldehydes derived from privileged heterocyclic scaffolds, such as furan, thiophene, and pyridine, to probe interactions with specific hydrophobic or hydrogen-bonding domains in the biological target.[8,17-19] All target **D** were purified by recrystallization or column chromatography and their structures were unequivocally confirmed by ^{1}H NMR, ^{13}C NMR, and high-resolution mass spectrometry (HRMS). The physical and spectroscopic data for all new compounds are provided in the Experimental Section.

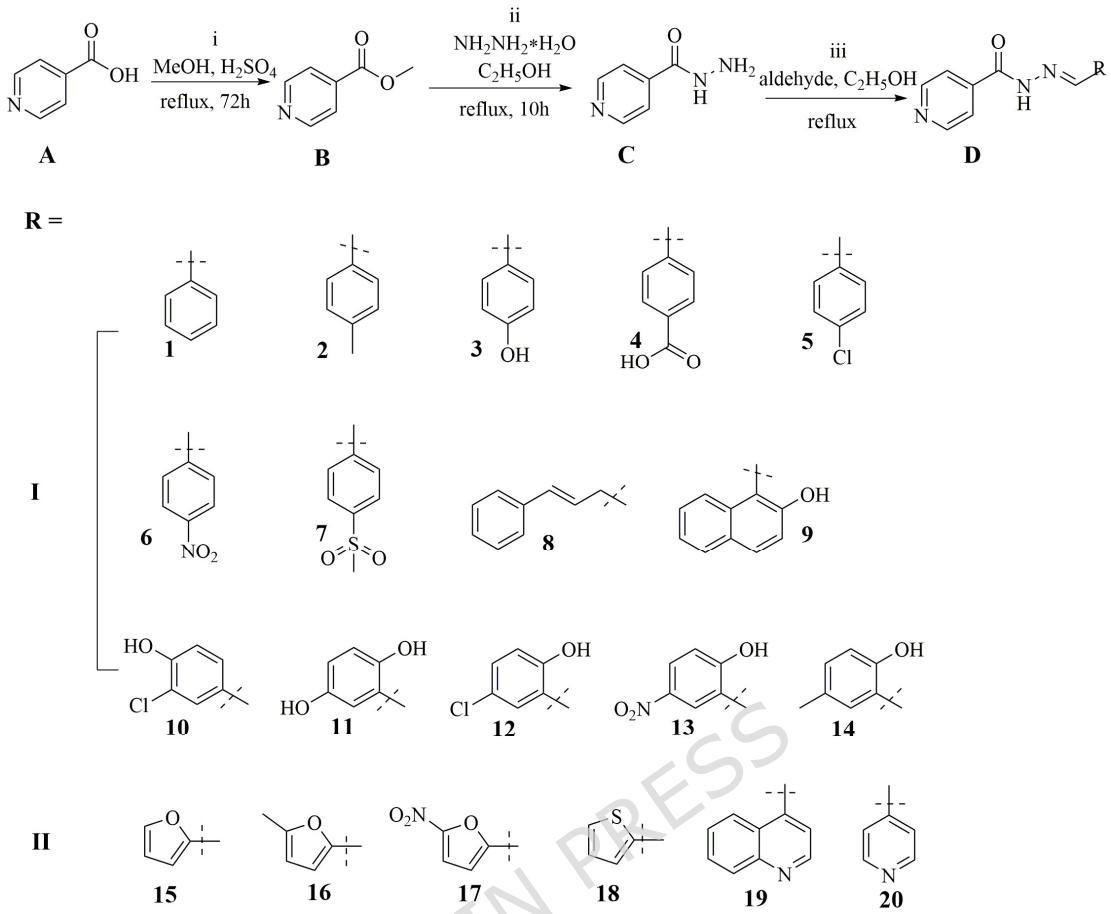

Scheme 2. Synthesis of isonicotinoyl hydrazone derivatives.
Conditions and reagents: (i) H_2SO_4, MeOH, reflux, 72 h, 88%; (ii) $NH_2NH_2{\cdot}H_2O$ and C_2H_5OH, reflux, 10h, 68%; (iii) Different aldehyde compounds, C_2H_5OH, reflux, yield 51% - 93%.

2.2. Biological activities

2.2.1. Antioxidant activity

H_2O_2 can generate hydroxyl radicals through redox reactions, inducing oxidative modifications related to the cytoplasm and lesions of AD neurons, which is consistent with the chronic dysregulation of metal ion binding in the cytoplasm of AD pyramidal neurons.[20] Determination of *in vitro* antioxidant activity of acylhydrazone using DPPH (1,1-diphenyl-2-picrylhydrazone) at 100 μM.[21] DPPH free radicals indirectly reflect the content and activity of antioxidant substances in the sample by measuring the residual DPPH free radical content after reacting with the analyte sample. DPPH free radicals can also be used to screen for antioxidants with high antioxidant activity and for the discovery of novel antioxidants. DPPH free radicals can also be used to study the mechanisms and kinetic processes of redox reactions, helping to gain a deeper understanding of the biochemical reactions in which free radicals participate. Antioxidants can provide protection for nerve cells and reduce the occurrence of neurodegenerative diseases. It can prevent oxidative damage to nerve cells by free radicals, thereby protecting the function of the nervous system. **8-12** and **19** have good ability to scavenge free radicals, and the

relevant data are listed in **Table 1**.

Table 1. AChE and MPO inhibitory activities and antioxidant capacity of Isonicotinoyl hydrazone derivatives (DPPH determination).

Compound	DPPH scavenger (% at 100 μM)	MPO inhibition (% at 10 μM)	AChE inhibition (% at 100 μM)
1	17.3 ± 0.4	7.2 ± 0.5	11.3 ± 0.5
2	13.5 ± 1.5	23.4 ± 0.9	12.5 ± 0.3
3	7.6 ± 1.4	9.5 ± 0.4	8.3 ± 0.4
4	17.4 ± 1.7	9.2 ± 0.7	7.4 ± 0.6
5	16.1 ± 0.2	6.3 ± 0.5	6.1 ± 0.3
6	9.3 ± 0.3	7.3 ± 0.4	7.3 ± 0.4
7	15.1 ± 0.2	55.1 ± 0.3	5.1 ± 0.5
8	90.5 ± 1.7	20.5 ± 0.6	10.5 ± 0.7
9	**93.6 ± 1.8**	**90.3 ± 0.8**	**73.6 ± 1.3**
10	95.7 ± 2.3	15.7 ± 1.3	15.7 ± 2.3
11	88.5 ± 2.7	98.5 ± 1.3	18.5 ± 2.4
12	99.3 ± 3.4	97.3 ± 2.2	19.3 ± 0.4
13	27.1 ± 0.9	97.1 ± 0.9	17.1 ± 0.8
14	21.1 ± 1.7	93.1 ± 1.7	21.1 ± 1.7
15	17.1 ± 0.8	34.1 ± 0.6	27.1 ± 0.8
16	15.1 ± 0.7	35.1 ± 0.6	25.1 ± 0.8
17	20.1 ± 1.1	87.1 ± 1.3	10.1 ± 0.3
18	13.1 ± 0.4	9.1 ± 0.3	23.1 ± 0.5
19	86.1 ± 0.6	76.1 ± 0.6	55.1 ± 0.7
20	17.1 ± 1.4	9.1 ± 0.3	18.1 ± 0.6
Isoniazid	87.1 ± 1.5	98.0± 2.8	5.1 ± 0.5

2.2.2. Myeloperoxidase inhibitory activity

Peroxisome abnormalities have a significant impact on neuronal function, and studies have shown that peroxisomes are closely related to the occurrence of Alzheimer's disease.[22] The inhibitory effects of all acylhydrazones on the chlorination activity of commercial recombinant rat MPO were evaluated by measuring the formation of *N*-monochlorotaurine. The inhibition rate of isoniazid derivatives on MPO at 10 μM was summarized in **Table 1** using isoniazid as a positive control. We found that **9, 11-14, 17,** and **19** showed potent inhibitory activity against myeloperoxidase, with inhibition rates of over 90% for **9** and **11-14**.

2.2.3. Acetylcholinesterase inhibitory activity and Multi-target SAR Analysis

The inhibitory activities of isonicotinoyl hydrazone derivatives (**1-20**) against AChE were detected using the Ellman's method, and their antioxidant capacities and MPO inhibitory effects were summarized in **Table 1**. Our SAR analysis reveals that AChE potency is primarily driven by the substituent volume and lipophilicity of the R group. Specifically, the inhibition rates of **9** (73.6%) and **19** (55.1%) at 100 μM were superior to the positive control Isoniazid and stood in sharp contrast to the

polar analogs (e.g., **3**, **4**, **10**-**14**), which mostly displayed inhibition below 30%. This potency is attributed to their large, planar bicyclic systems facilitating optimal hydrophobic filling and π-π stacking within the AChE gorge, a mechanism further supported by molecular docking demonstrating the necessity of a rigid hydrophobic anchor for maximum potency. Regarding redox-modulating activity, a distinct electronic trend emerged: electron-donating groups (EDG), particularly the poly-hydroxyl substitutions in **10**-**14**, dramatically enhanced antioxidant capacity and MPO inhibition by stabilizing radical intermediates. Conversely, electron-withdrawing groups (EWG), such as the nitro (**6**, **17**) or carboxyl (**4**) moieties, significantly diminished these effects. Notably, while the poly-hydroxyl series offered superior MPO inhibition, their excessive polarity hindered effective AChE binding. In contrast, **9** demonstrated a unique "pharmacological balance" by integrating the electron-donating capability of the hydroxyl group with the high lipophilicity of the naphthalene ring.

Given these screening results, we focused subsequent quantitative analysis on the two most potent candidates, **9** and **19**, by determining their IC_{50} values (**Table 2**). The quantitative data confirmed that while **19** possesses DPPH and MPO inhibitory potencies (IC_{50} = 30.1 and 8.1 μM) comparable to Isoniazid (IC_{50} = 27.1 and 7.1 μM), **9** exhibited significantly lower IC_{50} values in all assays. Specifically, the IC_{50} values of **9** for DPPH scavenging (13.3 μM) and MPO inhibition (0.9 μM) were approximately 2-fold and 8-fold more potent than those of Isoniazid, respectively. Therefore, based on this exceptional multi-target profile and the optimized balance of electronic and steric properties, **9** was selected as the lead candidate for all subsequent metal-chelating and neuroprotective investigations.

Table 2. IC_{50} values of the most active Isonicotinoyl hydrazone derivatives in MPO and DPPH assays.

Compound	DPPH scavenger IC_{50} (μM) (95% CI)	MPO inhibition IC_{50} (μM) (95% CI)
9	13.3 (11.8 – 14.8)	0.9 (0.78 – 1.02)
19	30.1 (26.6 – 33.6)	8.1 (7.3 – 8.9)
Isoniazid	27.1 (24.9 – 29.3)	7.1 (5.1 – 9.1)

2.2.4. Metal-chelating properties of 9

According to the amyloid cascade hypothesis, we can assume that the proteolytic processing of amyloid precursor protein (APP) leading to the accumulation of beta amyloid (Aβ) substances is the primary cause. During the pathological process, the accumulation of some metal ions such as copper (II) ions, iron (II) ions, and zinc (II) ions can exacerbate the condition. Therefore, we investigated the chelating ability of **9** towards metal Cu^{2+}, Fe^{2+}, Mg^{2+}, and Zn^{2+} ions, The results are shown in **Figure 1**. Consistent with our structural design, **9** exhibited a robust chelating efficiency exceeding 60% for all tested ions, indicating a significant potential to modulate metal dyshomeostasis. We speculate that this chelating effect is related to the coordination mode of the compound with metal ions. One possible mechanism is shown in **Figure 1**, the hydrazone nitrogen and the

adjacent ortho-hydroxyl group in **9** act as a bidentate ligand, forming highly stable chelate rings with these metal ions.

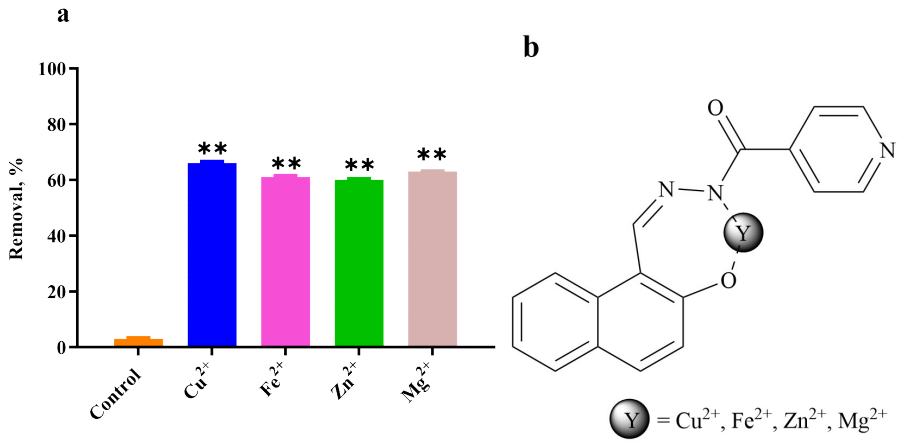

Figure 1.(a) Removal rate of metal ions by compound 9. (b) Binding mode diagram of 9 with metal ions. Data are presented as means ± SD (n = 3). (c)*p < 0.05, **p < 0.001 versus control group.

2.2.5. Cell protective effect of 9

Extracellular Aβ deposition is also one of the pathological features of AD, which may lead to neurotoxicity. Therefore, Aβ-induced PC12 cell models are commonly used to simulate the occurrence of neurotoxicity *in vitro*. We utilized Aβ42, as it is the predominant and more neurotoxic Aβ species found in AD plaques and exhibits faster aggregation kinetics than Aβ40.[23] As shown in **Figure 2(a)**, PC12 cells induced by Aβ42 were treated with different concentrations of **9**, and cell viability increased in a concentration dependent manner. Next, in SH-SY5Y cells, an Okadaic Acid (OA) induced cell model was applied to simulate tau hyperphosphorylation. Similarly, when OA induced SH-SY5Y cells were treated with different concentrations of **9**, as shown in **Figure 2(b)**, cell viability was enhanced in a concentration dependent manner. Finally, PHF6 induced PC12 cells were used to simulate tau aggregation mediated neurotoxicity *in vitro*. Similarly, when treated with different concentrations of **9**, cell viability significantly increased in a concentration dependent manner, as shown in **Figure 2(c)**. These results indicate that **9** can significantly improve the cell viability of these neuronal damage models and prevent cell death in a concentration dependent manner.

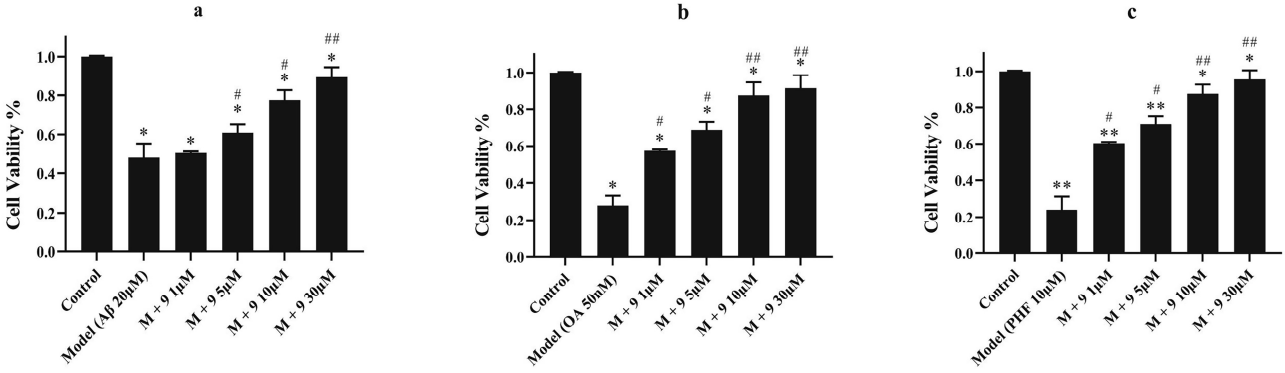

Figure 2. Neuroprotective effects of **9** on (a) Aβ42 induced PC12 cells, (b) OA induced SH-SY5Y cells, (c) PHF6 induced PC12 cells were shown. Data are presented as mean ± SD from three independent experiments (n = 3). Error bars represent standard deviation (SD). Difference is considered significant at $^{*}p < 0.05$, $^{**}p < 0.001$, *vs*. control group; $^{\#}p < 0.05$, $^{\#\#}p < 0.001$, *vs*. model group.

2.2.6. The effect of 9 on ROS

According to reports, oxidative stress is associated with tau phosphorylation and Aβ induction, which may ultimately lead to neuronal death.[1] Similarly, toxic peptides can also exacerbate oxidative stress levels. To evaluate the effect of **9** on oxidative stress induced by Aβ42 and PHF6, ROS levels were tested in this study. As shown in **Figure 3**, after incubation for 4 hours in PC12 cell models induced by Aβ42 (20 μM) or PHF6 (2.5 μM), intracellular ROS levels significantly increased, indicating that toxic peptides can induce oxidative stress. Interestingly, after treatment with **9**, ROS levels significantly decreased in a concentration dependent manner, indicating that **9** can reduce oxidative stress.

We hypothesize that this activity is primarily driven by direct radical quenching facilitated by the molecule's chemical structure. Specifically, the isonicotinoyl hydrazone moiety serves as the main active site. The N-H bond of the hydrazone is chemically prone to donate a hydrogen atom (H) to highly reactive ROS (such as hydroxyl radicals), following a hydrogen atom transfer (HAT) mechanism. This process stabilizes the ROS while forming a resonance-stabilized radical intermediate on **9**, thereby effectively terminating the free radical chain reaction.[12] This intrinsic structural feature provides a clear, mechanistic rationale for the observed reduction in cellular oxidative stress.

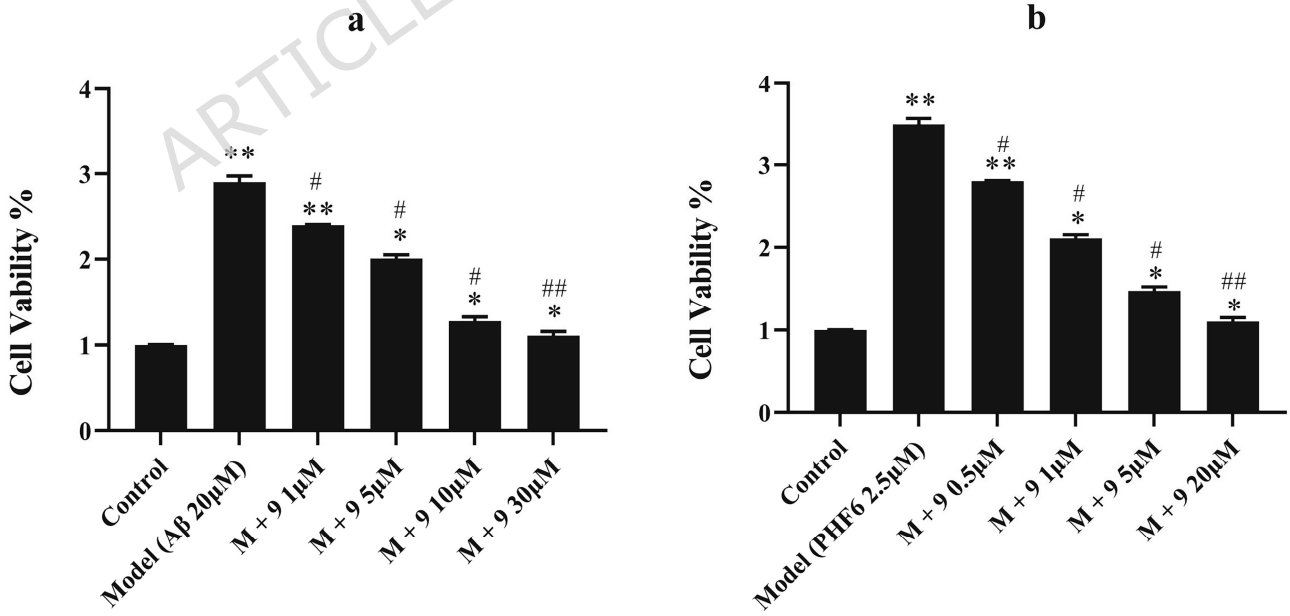

Figure 3. The effect of **9** on intracellular ROS levels induced by (a) Aβ42 and (b) PHF6 in PC12 cells. Data are presented as mean ± SD from three independent experiments (n = 3). Error bars represent standard deviation (SD). Difference is considered significant at $^{*}p < 0.05$, $^{**}p < 0.001$, *vs*. control group; $^{\#}p < 0.05$, $^{\#\#}p < 0.001$, *vs*. model group.

2.2.7. Molecular docking studies

To elucidate the structural basis underlying the remarkable inhibitory activity of **9** against AChE and MPO, molecular docking studies were conducted to predict its binding mode and key interactions with the target enzymes. For AChE (**Figure 4a and 4b**), **9** exhibited strong binding affinity, with a calculated binding energy of −8.0 kcal/mol. Notably, the predicted docking pose suggested a dual-binding mode that provides a plausible structural explanation for its inhibitory activity.

The planar naphthalene core of **9** is deeply embedded within the active-site gorge, where it establishes *π–π* stacking interactions with aromatic residues in the CAS, along with extensive hydrophobic contacts that stabilize the complex. Simultaneously, the hydrazide moiety extends toward the peripheral anionic site (PAS), forming hydrogen-bond interactions with nearby glutamine and tyrosine residues. This simultaneous engagement of both the CAS and PAS is expected to partially occlude the catalytic gorge and hinder substrate (acetylcholine) access, thereby contributing to the observed inhibitory effect.

In the case of MPO (**Figure 4c and 4d**), **9** demonstrated a favorable binding energy of −5.9 kcal/mol and adopted a well-accommodated conformation within the substrate-binding cavity proximal to the heme prosthetic group. Key stabilizing interactions include hydrogen bonds with glycine and asparagine residues, complemented by hydrophobic interactions with surrounding residues. This binding mode suggests that **9** may function as a cavity-blocking agent, potentially competing with hydrogen peroxide for access to the active site, thereby providing a structural basis for its inhibitory activity against MPO.

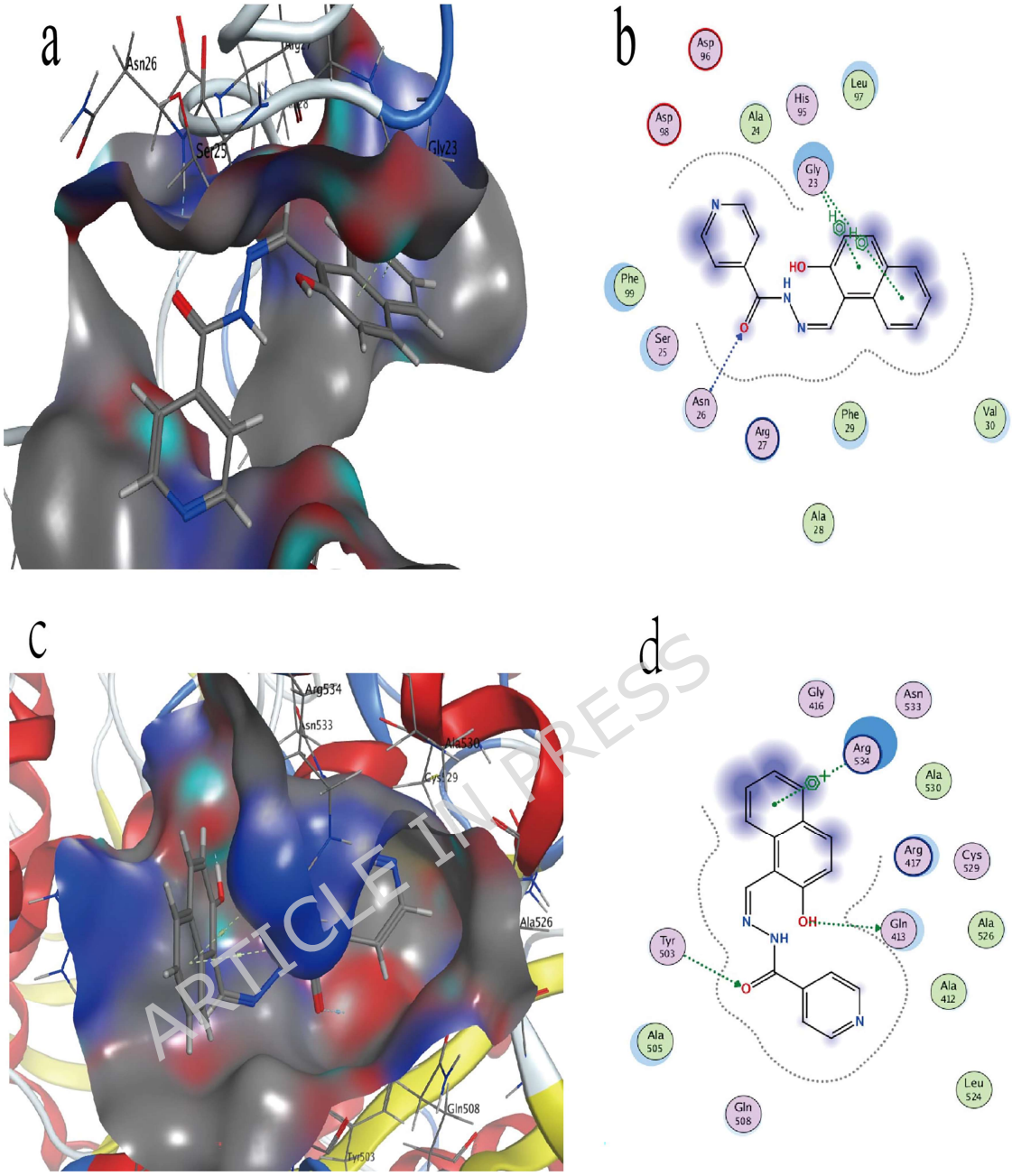

Collectively, these docking results indicate favorable binding interactions of **9** with both AChE and MPO and offer a plausible mechanistic model to support its dual inhibitory activity, in good agreement with the experimental observations.

Figure 4. 3D (a) and 2D (b) AChE (PDB code: 4M0E) docking with **9**. 3D (c) and 2D (d) MPO (PDB code: 4C1M) docking with **9**.

Conclusion

However, it should be noted that the present study is limited to *in vitro* evaluations. While **9** demonstrated significant multi-target potency and cytoprotective effects in cell models, its pharmacokinetic profile, blood-brain barrier (BBB) permeability, and *in vivo* efficacy remain to be further validated in animal models of Alzheimer's disease. Future studies will focus on

these aspects to fully assess its clinical translational potential. In summary, **9** is the only isonicotinoyl hydrazone derivative that exhibits significant activity against AD targets. Our SAR analysis reveals that its exceptional multi-target profile is fundamentally driven by the 2-hydroxynaphthyl moiety, which provides a unique structural synergy: the extended *π*-conjugated naphthalene ring ensures optimal hydrophobic filling and π-π stacking within enzyme gorges, while the electron-donating hydroxyl group significantly enhances radical-stabilizing capacity. These structural advantages endow **9** with potent multi-target activity against core AD pathological targets, particularly with a DPPH scavenging efficiency of 93% at 100 μM and an IC_{50} of 13 μM for DPPH; the inhibition rate of MPO reached 90% at 100 μM, and the IC_{50} for MPO was 0.9 μM; the inhibition of AChE reached 73% at 100 μM, outperforming its simpler analogs owing to its optimized lipophilic-electronic balance. Moreover, **9** has better chelating properties for biological metals (Cu^{2+}, Fe^{2+}, Mg^{2+}, Zn^{2+} ions), further validating the rational design of its multifunctional scaffold. Furthermore, in neuronal damage models, it significantly enhances cell viability and reduces oxidative stress levels. Docking studies corroborated the SAR findings, showing important complementary features in the interaction between the SAR-optimized molecule and the active sites of AChE and MPO.

Overall, the structural superiority identified through our SAR study makes **9** a promising lead candidate for the treatment of AD that merits further in-depth investigation.

4. Experimental section

4.1 Chemically synthetical experiments

The target compounds were fully characterized by ^1H and ^{13}C NMR spectroscopy. Chemical shifts (δ) are reported in ppm relative to the residual solvent signals of DMSO-d_6 (2.50 ppm for ^1H NMR and 39.50 ppm for ^{13}C NMR). The purity of all final compounds was confirmed to be greater than 95% by HPLC analysis on an Agilent 1100 system equipped with a Welch Ultimate C18 column (4.6 × 250 mm, 5 μm) maintained at 40 °C. The mobile phase consisted of 0.1% H_3PO_4 in water and acetonitrile at a flow rate of 1.0 mL/min with UV detection at 254 nm. Gradient elution was performed from 5% to 90% acetonitrile over 0–30 min.

Methyl Isonicotinate (**B**)

Isonicotinic acid (**A**) (1.0 mmol, 123 mg) was dissolved in anhydrous methanol (15 mL) in a round-bottom flask equipped with a magnetic stir bar. Concentrated sulfuric acid (0.5 mL, catalytic) was added dropwise to the stirred solution. The reaction mixture was heated under reflux with vigorous stirring for 72 hours, and the reaction progress was monitored by thin-layer chromatography (TLC). After completion, the reaction was cooled to room temperature and the majority of the methanol was removed under reduced pressure using a rotary evaporator. The resulting crude residue was diluted with water (20 mL) and transferred to a separatory funnel. The aqueous mixture was washed with ethyl acetate (3 × 15 mL) to remove non-acidic impurities. The aqueous phase was then carefully neutralized to pH 7-8 by the slow addition of a saturated aqueous sodium bicarbonate solution, with careful venting to release CO_2. The neutralized aqueous solution was extracted with ethyl acetate (3 × 20 mL). The combined organic extracts from this second extraction were washed with brine (20 mL), dried over anhydrous sodium sulfate (Na_2SO_4), and filtered. The filtrate was concentrated under reduced pressure to afford the crude product as a pale-yellow solid. The crude material was further

purified by flash column chromatography on silica gel to yield the pure title **B** as a white solid.

^{1}H NMR (400 MHz, DMSO-d_6) δ 8.73 (d, *J* = 6.0 Hz, 2H), 7.72 (d, *J* = 6.1 Hz, 2H), 3.83 (s, 3H). ^{13}C NMR (100 MHz, DMSO-d_6) δ 151.06, 137.10, 122.85, 52.96.

Isonicotinohydrazide (**C**)

B (1.0 mmol, 138 mg) was dissolved in absolute ethanol (15 mL) in a round-bottom flask equipped with a magnetic stir bar. To this solution, hydrazine monohydrate (2.0 mmol, 0.1 mL) was added dropwise. The reaction mixture was stirred vigorously and heated under reflux for 10 hours, with the reaction progress monitored by thin-layer chromatography (TLC). Upon completion, the reaction was cooled to room temperature. The mixture was then transferred to a separatory funnel and diluted with a saturated sodium chloride (brine) solution (20 mL). The aqueous layer was extracted with ethyl acetate (3 × 20 mL). The combined organic extracts were washed with an additional portion of brine (20 mL), dried over anhydrous sodium sulfate (Na_2SO_4), and filtered. The filtrate was concentrated under reduced pressure using a rotary evaporator to afford a crude solid. The product was further purified by flash column chromatography on silica gel to yield the pure title **C** as a white crystalline solid.

(*E*)-*N*'-Benzylideneisonicotinohydrazide (**1**)

C (1.0 mmol, 137 mg) was dissolved in absolute ethanol (15 mL) in a round-bottom flask equipped with a magnetic stir bar. Benzaldehyde (1.0 mmol, 0.10 mL) was added, followed by the addition of a catalytic amount of dilute hydrochloric acid. The reaction mixture was stirred at room temperature for 10 hours, during which the formation of a precipitate was typically observed. The reaction progress was monitored by thin-layer chromatography (TLC). Upon completion, the reaction was quenched by the addition of a saturated sodium chloride (brine) solution (20 mL). The resulting mixture was transferred to a separatory funnel. The product was extracted with ethyl acetate (3 × 20 mL). The combined organic extracts were washed with brine (20 mL), dried over anhydrous sodium sulfate (Na_2SO_4), filtered, and concentrated under reduced pressure using a rotary evaporator. The resulting crude solid was purified by flash column chromatography on silica gel to afford the pure title **1** as a white solid.

Yield: 209.3 mg (93%), 97.43% HPLC purity. ^{1}H NMR (400 MHz, DMSO-d_6) δ 12.38 (s, 1H, NH), 8.85 (d, *J* = 5.9 Hz, 2H, Py-H-2,6), 8.60 (s, 1H, CH=N), 8.02 (d, *J* = 5.9 Hz, 2H, Py-H-3,5), 7.75 (d, *J* = 7.5 Hz, 2H, Ph-H-2,6), 7.45 (s, 3H, Ph-H-3,4,5). ^{13}C NMR (100 MHz, DMSO-d_6) δ 161.19 (C=O), 149.45 (Py-C-2,6), 148.82 (C=N), 142.01 (Py-C-4), 134.04 (Ph-C-1), 130.47 (Ph-C-4), 128.93 (Ph-C-2,6), 127.33 (Ph-C-3,5) 122.44 (Py-C-3,5).

(*E*)-*N*'-(4-Methylbenzylidene)isonicotinohydrazide (**2**)

Yield: 210.3 mg (88%), 95.38% HPLC purity. ^{1}H NMR (400 MHz, DMSO-d_6) δ 12.01 (s, 1H , NH), 8.78 (d, J = 5.7 Hz, 2H, Py-H-2,6), 8.45 (s, 1H, CH=N)), 7.83 (d, *J* = 5.8 Hz, 2H, Py-H-3,5), 7.64 (d, *J* = 7.9 Hz, 2H, Ph-H-2,6), 7.26 (d, *J* = 7.9 Hz, 2H, Ph-H-3,5), 2.32 (s, 3H, Ar-CH_3). ^{13}C NMR (100 MHz, DMSO-d_6) δ 162.00 (C=O), 150.75 (Py-C-2,6), 149.51 (C=N), 140.98 (Py-C-4), 140.71 (Ph-C-4), 131.78 (Ph-C-1), 129.92 (Ph-C-2,6), 127.71 (Ph-C-3,5), 122.97 (Py-C-3,5), 21.48 (Ar-CH_3).

(*E*)-*N*'-(4-Hydroxybenzylidene)isonicotinohydrazide (**3**)

Yield: 204.9 mg (85%), 96.17% HPLC purity. ^{1}H NMR (400 MHz, DMSO-d_6) δ 12.08 (s, 1H, NH), 8.83 (d, *J* = 6.0 Hz, 2H, Py-H-2,6), 8.43 (s, 1H, CH=N), 7.93 (d, *J* = 6.1 Hz, 2H, Py-H-3,5), 7.58 (d, *J* = 8.6 Hz, 2H, Ph-H-2,6), 6.87 (d, *J* = 8.6 Hz, 2H, Ph-H-3,5). ^{13}C NMR (100 MHz, DMSO-d_6) δ 161.49 (C=O), 160.86 (Ph-C-4, C-OH), 149.71 (Py-C-2,6), 149.22 (C=N), 141.85 (Py-C-4), 129.19 (Ph-C-2,6), 125.00 (Ph-C-1), 122.17 (Py-C-3,5), 115.87 (Ph-C-3,5).

(*E*)-4-((2-Isonicotinoylhydrazono)methyl)benzoic acid (**4**)

Yield: 220.6 mg (82%), 97.31% HPLC purity. ^{1}H NMR (400 MHz, DMSO-d_6) δ 12.44 (s, 1H, NH or COOH), 8.85 (d, *J* = 6.0 Hz, 2H Py-H-2,6), 8.59 (s, 1H, CH=N)), 8.00 (dd, *J* = 12.6, 7.2 Hz, 3HPy-H-3,5 + Ph-H-2,6), 7.86 (d, *J* = 8.3 Hz, 2H, Ph-H-3,5). ^{13}C NMR (100 MHz, DMSO-d_6) δ 166.92(COOH), 161.28(C=O), 148.58 (Py-C-2,6), 148.26(C=N), 142.22 (Py-C-4), 138.03 (Ph-C-4), 132.10 (Ph-C-1), 129.89 (Ph-C-2,6), 127.40 (Ph-C-3,5), 122.63 (Py-C-3,5).

(*E*)-*N*'-(4-Chlorobenzylidene)isonicotinohydrazide (**5**)

Yield: 230.5 mg (89%), 96.31% HPLC purity. ^{1}H NMR (400 MHz, DMSO-d_6) δ 12.30 (s, 1H, NH), 8.83 (d, *J* = 6.1 Hz, 2H, Py-H-2,6), 8.52 (s, 1H, CH=N), 7.93 (d, *J* = 6.1 Hz, 2H, Py-H-3,5), 7.77 (d, *J* = 8.5 Hz, 2H, Ph-H-2,6), 7.53 (d, *J* = 8.5 Hz, 2H, Ph-H-3,5). ^{13}C NMR (100 MHz, DMSO-d_6) δ 161.40 (C=O), 149.42 (Py-C-2,6, 147.92 (C=N), 141.34 (Py-C-4), 134.91 (Ph-C-1), 132.97 (Ph-C-4), 129.03 (Ph-C-2,6), 122.28 (Py-C-3,5).

(*E*)-*N*'-(4-Nitrobenzylidene)isonicotinohydrazide (**6**)

Yield: 237.6 mg (88%), 98.26% HPLC purity. ^{1}H NMR (400 MHz, DMSO-d_6) δ 12.59 (s, 1H, NH), 8.86 (d, *J* = 6.1 Hz, 2H, Py-H-2,6), 8.65 (s, 1H, CH=N), 8.30 (d, *J* = 8.7 Hz, 2H, Ph-H-3,5), 8.00 (d, *J* = 9.0 Hz, 4H, Py-H-3,5 + Ph-H-2,6). ^{13}C NMR (100 MHz, DMSO-d6) δ 161.49 (C=O), 148.92 (Py-C-2,6), 148.09 (C=N), 146.83 (Ph-C-4), 141.65 (Py-C-4), 140.25 (Ph-C-1), 128.26 (Ph-C-2,6),, 124.12 (Ph-C-3,5), 122.43.(Py-C-3,5).

(E)-N'-(4-(Methylsulfonyl)benzylidene)isonicotinohydrazide (**7**)

Yield: 212.1 mg (70%), 95.13% HPLC purity. ^{1}H NMR (400 MHz, DMSO-d_6) δ 12.50 (s, 1H, NH), 8.85 (d, *J* = 6.1 Hz, 2H, Py-H-2,6), 8.63 (s, 1H, CH=N), 8.01 - 7.915 (m, 6H, Py-H-3,5 + Ph-H-2,6 + Ph-H-3,5)), 3.27 (s, 3H, -SO_2CH_3). ^{13}C NMR (100 MHz, DMSO-d_6) δ 161.63 (C=O), 149.39 (Py-C-2,6), 147.31 (C=N), 141.74 (Py-C-4), 141.25 (Ph-C-1), 138.80 (Ph-C-4), 127.94 (Ph-C-2,6), 127.60(Ph-C-3,5), 122.18 (Py-C-3,5), 43.44(-SO_2CH_3).

(*E*)-*N*'-((*E*)-3-Phenylallylidene)isonicotinohydrazide (**8**)

Yield: 183.2 mg (73%), 95.44% HPLC purity. ^{1}H NMR (400 MHz, DMSO-d_6) δ 12.12 (s, 1H, NH), 8.82 (d, *J* = 6.1 Hz, 2H, Py-H-2,6), 8.32 (d, *J* = 8.4 Hz, 1H, CH=N), 7.92 (d, *J* = 6.0 Hz, 2H , Py-H-3,5), 7.63 (d, *J* = 7.2 Hz, 2H, Ph-H-2,6), 7.36 (dt, *J* = 24.7, 7.2 Hz, 3H, Ph-H-3,4,5), 7.09 (d, *J* = 6.5 Hz, 2H, -CH=CH-Ph). ^{13}C NMR (100 MHz, DMSO-d_6) δ = 161.41 (C=O), 151.43 (C=N), 149.37 (Py-C-2,6), 141.55 (Py-C-4), 140.03 (-CH=CH-Ph), 136.02 Ph-C-1), 129.26 (Ph-C-4), 127.46 (Ph-C-2,6), 125.39 (Ph-C-3,5), 122.25 (Py-C-3,5).

(*E*)-*N*'-((2-Hydroxynaphthalen-1-yl)methylene)isonicotinohydrazide (**9**)

Yield: 232.8 mg (80%), 97.57% HPLC purity.^{1}H NMR (400 MHz, DMSO-d_6) δ 12.60 (s, 1H, NH), 9.58 (s, 1H, OH), 8.87 (d, *J* = 5.9 Hz, 2H, Py-H-2,6), 8.33 (d, *J* = 8.6 Hz, 1H, Naph-H-3), 8.00 – 7.88 (m, 4H, Py-H-3,5 + Naph-H-5,8)), 7.62 (t, *J* = 7.6 Hz, 1H, Naph-H-7), 7.41 (t, *J* = 7.4 Hz, 1H, Naph-H-6)), 7.24 (d, *J* = 8.9 Hz, 1H, Naph-H-4). ^{13}C NMR (100 MHz, DMSO-d_6) δ 160.59 (C=O), 158.46 (Naph-C-2, C-OH), 149.64 (Py-C-2,6), 148.24 (C=N), 140.91 (Py-C-4), 133.19 (Naph-C-10), 131.65 (Naph-C-9), 129.01 (Naph-C-5), 127.88 (Naph-C-8), 123.79 (Naph-C-4), 121.95 (Naph-C-3), 121.22 (Naph-C-6), 118.17 (Naph-C-7), 108.017 (Naph-C-1). HRMS (ESI) m/z: $[M + Na]^+$ Calcd for $C_{17}H_{14}N_3O_2Na$ 314.0905; Found 314.0903.

(***E***)-*N*'-(3-Chloro-4-hydroxybenzylidene)isonicotinohydrazide (**10**)

Yield: 206.2 mg (75%),95.52% HPLC purity. ^{1}H NMR (400 MHz, DMSO-d_6) δ 12.08 (s, 1H, NH), 8.80 (d, *J* = 5.9 Hz, 2H, Py-H-2,6), 8.38 (s, 1H, CH=N), 7.87 (d, *J* = 6.0 Hz, 2H, Py-H-3,5), 7.73 (s, 1H, Ph-H-2), 7.55 (d, *J* = 10.3 Hz, 1H, Ph-H-6), 7.07 (d, *J* = 8.4 Hz, 1H, Ph-H-5). ^{13}C NMR (100 MHz, DMSO-d_6) δ 161.45 (C=O), 155.27 (Ph-C-4, C-OH), 149.97 (Py-C-2,6), 148.17 (C=N), 141.13 (Py-C-4), 128.72 (Ph-C-1), 127.63 (Ph-C-6), 126.42 (Ph-C-2), 121.84 (Py-C-3,5), 120.53 (Ph-C-3), 116.98 (Ph-C-5).

(*E*)-*N*'-(2,5-Dihydroxybenzylidene)isonicotinohydrazide (**11**)

Yield: 200.5 mg (78%), 95.94% HPLC purity. ^{1}H NMR (400 MHz, DMSO-d_6) δ 12.29 (s, 1HNH), 8.80 (d, *J* = 5.9 Hz, 2HPy-H-2,6), 8.66 (s, 1H CH=N), 7.90 (d, *J* = 6.0 Hz, 2HPy-H-3,5), 7.05 (s, 1H, Ph-H-6), 6.78 (s, 2H, Ph-H-3 + Ph-H-4). ^{13}C NMR (100 MHz, DMSO-d_6) δ 161.29 (C=O), 150.49 (Ph-C-2, C-OH), 150.08 (Ph-C-5, C-OH), 149.90 (Py-C-2,6), 148.76 (C=N), 140.79 (Py-C-4), 121.94 (Py-C-3,5), 119.55 (Ph-C-1), 119.10 (Ph-C-6), 117.34 (Ph-C-4), 113.67 (Ph-C-3).

(*E*)-*N*'-(5-Chloro-2-hydroxybenzylidene)isonicotinohydrazide (**12**)

Yield: 214.5 mg (78%), 95.42% HPLC purity. ^{1}H NMR (400 MHz, DMSO-d_6) δ 12.49 (s, 1H, NH), 8.82 (d, *J* = 6.1 Hz, 2H, Py-H-2,6), 8.70 (s, 1H, CH=N), 7.93 (d, *J* = 6.1 Hz, 2H, Py-H-3,5), 7.65 (s, 1H, Ph-H-6), 7.28 (d, *J* = 11.5 Hz, 1H, Ph-H-4), 6.95 (d, *J* = 8.8 Hz, 1H, Ph-H-3). ^{13}C NMR (100 MHz, DMSO-d_6) δ 161.31 (C=O), 156.25 (Ph-C-2, C-OH), 149.61 (Py-C-2,6), 146.93 (C=N), 140.82 (Py-C-4), 131.17 (Ph-C-6), 127.42 (Ph-C-4), 123.15 (Ph-C-1), 122.11 (Py-C-3,5), 120.68 (Ph-C-5), 118.36 (Ph-C-3).

(*E*)-*N*'-(2-Hydroxy-5-nitrobenzylidene)isonicotinohydrazide (**13**)

Yield: 200.2 mg (70%), 98.91% HPLC purity. ^{1}H NMR (400 MHz, DMSO-d_6) δ 12.43 (s, 1H, NH), 8.76 (d, *J* = 23.0 Hz, 3H, Py-H-2,6 + Ph-H-6), 8.55 (s, 1H, CH=N), 8.12 (s, 1H, Ph-H-4), 7.86 (s, 2H, Py-H-3,5), 7.09 (s, 1H, Ph-H-3).^{13}C NMR (100 MHz, DMSO-d_6) δ 162.64 (C=O), 161.55 (Ph-C-2, C-OH), 150.13 (Py-C-2,6), 145.15 (C=N), 140.14 (Py-C-4), 139.97 (Ph-C-5), 126.84 (Ph-C-1), 123.48 (Ph-C-4), 121.73 (Py-C-3,5), 120.00 (Ph-C-6), 117.13 (Ph-C-3).

(*E*)-*N*'-(2-Hydroxy-5-methylbenzylidene)isonicotinohydrazide (**14**)

Yield: 204.1 mg (80%), 96.22% HPLC purity . ^{1}H NMR (400 MHz, DMSO-d_6) δ 12.65 (s, 1H, NH), 11.27 (s, 1H, OH), 9.15 (d, *J* = 5.8 Hz, 2H, Py-H-2,6), 9.00 (s, 1H, CH=N), 8.22 (d, *J* = 5.9 Hz, 2H, Py-H-3,5), 7.72 (s, 1H, Ph-H-6), 7.45 (d, *J* = 8.3 Hz, 1H, Ph-H-4), 7.20 (d, *J* = 8.3 Hz, 1H, Ph-H-3), 2.58 (s, 3H, Ar-CH_3). ^{13}C NMR (100 MHz, DMSO-d_6) δ 161.42 (C=O), 155.50 (Ph-C-2, C-OH), 150.40 (Py-C-2,6), 149.24 (C=N), 140.03 (Py-C-4), 132.49 (Ph-C-1), 129.28 (Ph-C-6), 128.06 (Ph-C-4), 122.59 (Py-C-3,5), 118.34 (Ph-C-3), 116.38 (Ph-C-5), 19.97 (Ar-CH_3).

(*E*)-*N*'-(Furan-2-ylmethylene) isonicotinohydrazide (**15**)

Yield: 114.0 mg (53%), 96.04% HPLC purity. ^{1}H NMR (400 MHz, DMSO-d_6) δ 12.52 (s, 1H, NH), 8.92 (d, *J* = 6.2 Hz, 2H, Py-H-2,6), 8.53 (s, 1H, CH=N), 8.14 (d, *J* = 6.3 Hz, 2H, Py-H-3,5), 7.88 (s, 1H, Furan-H-5), 7.00 (d, *J* = 3.4 Hz, 1H, Furan-H-3), 6.66 (s, 1H, Furan-H-4). ^{13}C NMR (100 MHz, DMSO-d_6). δ 160.37 (C=O), 149.09 (Py-C-2,6), 146.91 (C=N), 145.71 (Furan-C-2), 139.28 (Py-C-4), 123.36 (Furan-C-5), 114.66 (Furan-C-3), 112.37 (Furan-C-4).

(*E*)-*N*'-((5-Methylfuran-2-yl)methylene)isonicotinohydrazide (**16**)

Yield: 137.4 mg (60%), 97.19% HPLC purity. ^{1}H NMR (400 MHz, DMSO-d_6) δ 12.25 (s, 1H, NH), 8.84 (d, *J* = 5.9 Hz, 2H, Py-H-2,6), 8.37 (s, 1H, CH=N), 7.99 (d, *J* = 5.9 Hz, 2H, Py-H-3,5), 6.86 (s, 1H, Furan-H-3), 6.26 (s, 1H, Furan-H-4), 2.33 (s, 3H, Furan-CH_3). ^{13}C NMR (100 MHz, DMSO-d_6) δ 160.82 (C=O), 155.10 (Furan-C-5), 148.56 (Py-C-2,6), 147.62 (C=N), 142.18 (Py-C-4), 138.88 (Furan-C-2), 122.47 (Py-C-3,5), 116.41 (Furan-C-3), 108.78 (Furan-C-4), 13.52 (Furan-CH_3).

(*E*)-*N*'-((5-Nitrofuran-2-yl)methylene)isonicotinohydrazide (**17**)

Yield: 158.6 mg (61%), 96.39% HPLC purity. ^{1}H NMR (400 MHz, DMSO-d_6) δ 12.57 (s, 1H, NH), 8.82 (d, *J* = 5.7 Hz, 2H, Py-H-2,6), 8.47 (s, 1H, CH=N), 7.80 (d, *J* = 47.1 Hz, 3H, Py-H-3,5 + Furan-H-4), 7.31 (s, 1H, Furan-H-3). ^{13}C NMR (100 MHz, DMSO-d_6) δ 161.83 (C=O), 151.34 (Furan-C-5), 149.89 (Py-C-2,6), 140.43 (Py-C-4), 136.84 (C=N), 121.90 (Py-C-3,5), 116.06 (Furan-C-3), 114.55 (Furan-C-4).

(*E*)-*N*'-(Thiophen-2-ylmethylene)isonicotinohydrazide (**18**)

Yield: 138.6 mg (60%), 96.81% HPLC purity. ^{1}H NMR (400 MHz, DMSO-d_6) δ 12.04 (s, 1H, NH), 8.78 – 8.68 (m, 3H, Py-H-2,6 + CH=N), 7.80 (d, *J* = 5.9 Hz, 2H, Py-H-3,5), 7.69 (d, *J* = 5.0 Hz, 1H, Thiophene-H-5), 7.51 (d, *J* = 3.4 Hz, 1H, Thiophene-H-3), 7.13 (d, *J* = 8.6 Hz, 1H, Thiophene-H-4). ^{13}C NMR (100 MHz, DMSO-d_6) δ 161.51 (C=O), 150.34 (Py-C-2,6), 144.14 (C=N), 140.46 (Py-C-4), 138.78 (Thiophene-C-2), 131.58 (Thiophene-C-5), 129.46 (Thiophene-C-3), 127.97 (Thiophene-C-4), 121.52 (Py-C-3,5).

(*E*)-*N*'-(Quinolin-4-ylmethylene)isonicotinohydrazide (**19**)

Yield: 223.6 mg (81%), 98.56% HPLC purity. ^{1}H NMR (400 MHz, DMSO-d_6) δ 12.82 (s, 1H, NH), 9.33 (s, 1H, CH=N), 9.06 (d, *J* = 4.6 Hz, 1H, Quin-H-2), 8.85 (d, *J* = 5.7 Hz, 2H, Py-H-2,6), 8.75 (d, *J* = 8.4 Hz, 1H, Quin-H-8), 8.16 (d, *J* = 8.3 Hz, 1H, Quin-H-5), 8.01 – 7.78 (m, 5H, Py-H-3,5 + Quin-H-3,6,7). ^{13}C NMR (100 MHz, DMSO-d_6) δ 161.78 (C=O), 149.00

(Quin-C-2), 146.11 (C=N), 145.65 (Quin-C-4), 130.79 (Quin-C-8a), 128.32 (Quin-C-5), 127.95 (Quin-C-7), 124.90 (Quin-C-6), 124.46 (Quin-C-8), 121.99 (Py-C-3,5), 119.88 (Py-C-2,6 + Quin-C-3).

(*E*)-*N*'-(Pyridin-4-ylmethylene)isonicotinohydrazide (**20**)

Yield: 180.8 mg (80%), 95.62% HPLC purity. ^{1}H NMR (400 MHz, DMSO-d_6) δ 12.50 (s, 1H, NH), 8.80 (d, *J* = 5.4 Hz, 2H, Py1-H-2,6), 8.69 (d, *J* = 5.4 Hz, 2H, Py2-H-2,6), 8.54 (s, 1H, CH=N), 7.88 (d, *J* = 5.4 Hz, 2H, Py1-H-3,5), 7.74 (d, *J* = 5.4 Hz, 2H, Py2-H-3,5). ^{13}C NMR (100 MHz, DMSO-d_6) δ 160.44 (C=O), 148.21 (Py1-C-2,6), 142.59 (Py1-C-4), 126.96 (Py2-C-4), 123.31 (Py1-C-3,5), 122.91 (Py2-C-3,5), 114.31 (Py2-C-2,6), 109.71 (C=N).

4.2. Biological assays

4.2.1. Antioxidant activity assay

DPPH exhibits strong absorption at 517 nm, but upon reaction with antioxidants, the absorption peak disappears. Add 100 μL of isoniazid derived methanol solution (3-600 μM) to 100 μL of DPPH methanol solution (200 μM). After 30 minutes of static reaction, measure the remaining free radical DPPH at 517 nm at room temperature. Isoniazid was used as a positive control.[24]

4.2.2. MPO inhibition experiments

Commercial active recombinant rat MPO (Catalog No. UEPA601Ra61, Cloud-Clone Corp., Wuhan, China) was used to evaluate the MPO inhibitory activity of the compounds. The production of HOCl was measured by monitoring the formation of *N*-monochlorotaurine. Compounds **1-20** were dissolved in DMSO. The experiment was conducted in a 96-well plate with a final volume of 125 μL, consisting of taurine (10 mM), NaCl (100 mM), commercial MPO enzyme solution (final concentration of 20 nM), phosphate buffer solution (0.05 M, pH 7.4), and inhibitors (0.01-30 μM). The reaction was initiated by adding H_2O_2 (100 μM) and stopped after 20 minutes by adding catalase (40 μg/mL). Then, add 25 μL of colorimetric reagent (3,3', 5,5'-tetramethylbenzidine (TMB)/potassium iodide 100 μM) to detect the formed *N*-monochlorotaurine. After the blue color appears, add 100 μL of H_2SO_4 (1M) and measure the oxidized TMB at 450 nm.[25]

4.2.3. AChE inhibition experiments

Measure AChE inhibitory activity using a 96 well plate and spectrophotometry. Firstly, dissolve **1-20** in DMSO. Then incubate Ellman's reagent (acid 5,5'-dithiobis-(2-nitrobenzoate) (60 μM), pH 8 (0.05 M) phosphate buffer, inhibitor (100 μM), and E. electricus AChE (0.25U/mL) in a final volume of 250 μL for 40 minutes. Finally, acetylthiocholine iodide (1.5 mM) was added to initiate the reaction. Perform three parallel experiments on each compound and measure the absorbance at 412nm. Calculate the inhibition percentage by comparing the enzyme reaction rates between the sample and control groups. Use isoniazid as a positive control.[26]

4.2.4. Metal binding studies

After incubation at room temperature for 2 hours, record the UV absorption of test **9** (20 μM in DMSO) in the presence of $CuCl_2$, $FeCl_2$, $MgCl_2$, and $ZnCl_2$ (20 μM in DMSO) within the wavelength range of 200-600 nm. Determine the standard curves of **9**-$Fe^{2+}$and **9**-Zn^{2+} complexes by titrating 1 m (5-80 μM methanol) solution with

$FeCl_2$ and $ZnCl_2$ (20 μM methanol solution). After incubating at room temperature for 2 hours, record the UV spectra 400-375 nm and plot the mole fraction of the test compound by subtracting the corresponding concentrations of metal salts and the values of the test compound.[27]

4.2.5. Cell protective effect

(1) Cell viability can be evaluated using MTT assay. Highly differentiated PC12 cells (Catalog No. ZY-C6013R, Shanghai Zeye Biological Technology Co., Ltd.) were seeded in a 96-well plate at a density of 1×10^4 cells per well in 100 μL of RPMI 1640 culture medium. After 24 hours, with or without the addition of $A\beta_{42}$ peptide (20 μM) and different concentrations of **9**, the cells were cultured for another 24 hours. MTT (0.5 mg/mL) was added to each well, and the microplate was cultured for another 4 hours in a 37 °C incubator. The solution in each well was discarded and 100 μL of DMSO was added to completely dissolve the formazan Record the absorbance at 570 nm using a tablet reader (BioTek).

(2) For the cell viability of PHF6 in the PC12 cell model, a similar experimental method was used, except for using PHF6 peptide (2.5 μM) instead of Aβ42 peptide.

(3) The human neuroblastoma cell line SH-SY5Y (purchased from Shanghai Zeye Biological Technology Co., Ltd. Shanghai, China) cell-based model induced by OA was utilized to simulate tau hyperphosphorylation and cell death. Cultivate the cells into a 96 well plate, with approximately 4×10^4 cells per well in 100 μL of culture medium. After 24 hours, replace the culture medium with or without OA and different concentrations of **9**. As mentioned earlier, the survival rate of cells was evaluated through MTT assay.[28]

4.2.6. ROS check

PC12 cells induced by Aβ and PHF6 were seeded at a density of 5×10^4 cells/mL on a black transparent 96 well plate and grown 24h. Then remove the culture medium and add diluted DCFH-DA solution (30 μL/well). Cultivate the cells in a dark environment at 37 °C in a 5% CO_2 incubator for 20 minutes, and discard the culture medium. The cells were washed three times with serum-free culture medium, treated with **9** (1, 5, 10, 20 μM) and 20 μM DAP at 37 °C for 4 hours, and finally detected using a SpectraMAX M5 microplate analyzer with an Ex/Im of 485/535nm.[29]

4.2.7. Molecular docking studies

Molecular docking studies were performed using the Discovery Studio 2016 client. The structures of all Isonicotinoyl hydrazone derivatives (**1-20**)were constructed with ChemDraw 18.1 and subjected to energy minimization using the CHARMm force field. The three-dimensional crystal structures of AChE (PDB ID: 4M0E) and MPO (PDB ID: 4C1M) were retrieved from the RCSB Protein Data Bank. Both protein structures were prepared using the "Prepare Protein" tool, which involved removing water molecules, adding missing hydrogen atoms, and repairing incomplete amino acid side chains.

Docking simulations were executed via the CDOCKER program. The binding site spheres were defined based on the coordinates of the co-crystallized ligands. The docking protocol followed the standard parameters optimized for these targets, and binding energies (kcal/mol)

were calculated using the ‘In Situ Ligand Minimization’ and ‘Calculate Binding Energy’ protocols, providing a structural rationalization for the SAR of the target compounds.[8]

4.2.8 Statistical analysis

All experiments were independently repeated at least three times, with three replicate wells per experiment. Data are expressed as mean ± standard deviation (SD), as specified in the figure legends. Statistical analysis was performed using GraphPad Prism 9.0 software. Comparisons between two groups were analyzed by unpaired Student’s t-test, while comparisons among multiple groups were performed by one-way analysis of variance (ANOVA) followed by Tukey’s post hoc test. Significance was set at *$p < 0.05$ and **$p < 0.001$.

Funding： No funding was received for this research.

Ethical Approval: This study did not involve any human participants or animals. Therefore, ethical approval was not required for this study.

Reference

Scheltens, P. et al. Alzheimer's disease. *Lancet* **397,** 1577-1590 (2021).

Avila, J. & Perry, G. A multilevel view of the development of Alzheimer's disease. *Neuroscience* **457,** 283-293 (2021).

Hane, F. T., Lee, B. Y. & Leonenko, Z. Recent progress in Alzheimer's disease research, part 1: pathology. *J. Alzheimers Dis.* **57,** 1-28 (2017).

Knopman, D. S. et al. Alzheimer disease. *Nat. Rev. Dis. Primers* **10,** 42 (2024).

Bai, R., Guo, J., Ye, X. Y., Xie, Y. & Xie, T. Oxidative stress: the core pathogenesis and mechanism of Alzheimer's disease. *Ageing Res. Rev.* **77,** 101619 (2022).

Sankar, J., Chauhan, A., Singh, R. & Mahajan, D. Isoniazid: historical development, metabolism associated toxicity and a perspective on its pharmacological improvement. *Front. Pharmacol.* **15,** 1441147 (2024).

Frias, C. C. et al. Acylhydrazones derived from isonicotinic acid: synthesis, characterization, and evaluation against Alzheimer's disease biomarkers. *J. Mol. Struct.* **1312,** 138456 (2024).

Santos, D. C. et al. Acylhydrazones as isoniazid derivatives with multi-target profiles for the treatment of Alzheimer's disease: Radical scavenging, myeloperoxidase/acetylcholinesterase inhibition and biometal chelation. *Bioorg. Med. Chem.* **28,** 115470 (2020).

Singh, A., Kukreti, R., Saso, L. & Kukreti, S. Oxidative stress: a key modulator in neurodegenerative diseases. *Molecules* **24,** 1583 (2019).

Cipriano, A. et al. NADPH oxidases: from molecular mechanisms to current inhibitors in anticancer therapy. *J. Med. Chem.* **66,** 7926-7955 (2023).

Birben, E., Sahiner, U. M., Sackesen, C., Erzurum, S. & Kalayci, O. Oxidative stress and antioxidant defense. *World Allergy Organ. J.* **5,** 9-19 (2012).

Rivera Antonio, A. M., Padilla Martínez, I. I., Torres-Ramos, M. A. & Rosales-Hernández, M. C. Myeloperoxidase as a therapeutic target for oxidative damage in Alzheimer's disease. *J. Enzyme Inhib. Med. Chem.* **40,** 2456282 (2025).

Liu, Z., Zhou, T., Ziegler, A. C., Dimitrion, P. & Zuo, L. Oxidative stress in neurodegenerative diseases: from molecular mechanisms to clinical applications. *Oxid. Med. Cell. Longev.* **2017,** 2525967 (2017).

Bartolić, M., Matošević, A., Maraković, N. & Gašo-Sokač, D. Evaluation of hydrazone and N-acylhydrazone derivatives of vitamin B6 and pyridine-4-carbaldehyde as potential drugs against Alzheimer's disease. *J. Enzyme Inhib. Med. Chem.* **39,** 2431832 (2024).

Zou, D. et al. Latest advances in dual inhibitors of acetylcholinesterase and monoamine oxidase B against Alzheimer's disease. *J. Enzyme Inhib. Med. Chem*. **38,** 2270781 (2023).

Kondeva-Burdina, M., Krastev, K., Pencheva, T. & Angelova, V. T. Indole-based hydrazide-hydrazone and sulfonylhydrazone derivatives as MAO-B inhibitors with multitarget potential for neurodegenerative diseases. *Pharmacia* **72,** 1–13 (2025).

Siddiqui, S. M., Salahuddin, A. & Azam, A. Synthesis, characterization and antiamoebic activity of some hydrazone and azole derivatives bearing pyridyl moiety as a promising heterocyclic scaffold. *Eur. J. Med. Chem.* **49,** 411-416 (2012).

Judge, V. et al. Isonicotinic acid hydrazide derivatives: synthesis, antimicrobial activity, and QSAR studies. *Med. Chem. Res.* **21,** 1451-1470 (2012).

Alegaon, S. G., Alagawadi, K. R. & Dadwe, D. H. Synthesis and antitubercular activity of novel 3,5-diaryl-4,5-dihydro-1H-pyrazole derivatives. *Drug Res. (Stuttg)* **64,** 553-558 (2014).

Perluigi, M., Di Domenico, F. & Butterfield, D. A. Oxidative damage in neurodegeneration: roles in the pathogenesis and progression of Alzheimer disease. *Physiol. Rev.* **104,** 233–270 (2024).

Belkheiri, N. et al. Synthesis and antioxidant activity evaluation of a syringic hydrazones family. *Eur. J. Med. Chem.* **45,** 3019-3026 (2010).

Uzor, N. E., McCullough, L. D. & Tsvetkov, A. S. Peroxisomal dysfunction in neurological diseases and brain aging. *Front. Cell. Neurosci.* **14,** 44 (2020).

Yu, Y., Yu, S., Battaglia, G. & Tian, X. Amyloid-β in Alzheimer's disease: structure, toxicity, distribution, treatment, and prospects. *Int. J. Mol. Sci.* **25,** 10705 (2024).

Bitar, D. et al. Population-based analysis of invasive fungal infections, France. *Emerg. Infect. Dis.* **20,** 1149-1155 (2014).

Pattison, D. I., Hawkins, C. L. & Davies, M. J. What are the plasma targets of the oxidant hypochlorous acid? A kinetic modeling approach. *Free Radic. Biol. Med.* **212,** 345–358 (2024).

Baliyan, S. et al. Determination of antioxidants by DPPH radical scavenging activity and quantitative phytochemical analysis of Ficus religiosa. *Molecules* **27,** 1326 (2022).

Chen, W. et al. Therapeutic inhibition of MPO stabilizes pre-existing high risk atherosclerotic plaque. *Redox Biol.* **58,** 102532 (2022).

Cabral, R. G., Viegas, G., Pacheco, R., Sousa, A. C. & Robalo, M. P. Sustainable synthesis, antiproliferative and acetylcholinesterase inhibition of 1,4- and 1,2-naphthoquinone derivatives. *Molecules* **28,** 1232 (2023).

Dudev, T. & Lim, C. Metal binding affinity and selectivity in metalloproteins: Insights from computational studies. *Annu. Rev. Biophys.* **37,** 97-116 (2008).

Competing Interests

There are no conflicts to declare.

Data Availability Statement

All data generated or analysed during this study are included in this published article (and its Supplementary Information files).

Author Contributions Statement

ZW and KZ conceived and designed the study and supervised the overall research project.

YC and ZL carried out the chemical synthesis and structural characterization of the compounds.

BG and ZWg performed the biological activity assays, including enzyme inhibition and antioxidant experiments, and **ZWg** conducted the molecular docking studies.

XM conducted the cell-based experiments and analyzed the cytoprotective activity data.

ZW analyzed the data and drafted the manuscript.

All authors discussed the results, contributed to data interpretation, and reviewed and approved the final manuscript.